Understanding the role of ultra-thin polymeric interlayers in improving efficiency of polymer light emitting diodes

Jim Bailey, Edward N. Wright, Xuhua Wang, Alison B. Walker, Donal D. C. Bradley, and Ji-Seon Kim

Citation: Journal of Applied Physics **115**, 204508 (2014); doi: 10.1063/1.4879455
View online: http://dx.doi.org/10.1063/1.4879455
View Table of Contents: http://scitation.aip.org/content/aip/journal/jap/115/20?ver=pdfcov
Published by the AIP Publishing

Understanding the role of ultra-thin polymeric interlayers in improving efficiency of polymer light emitting diodes

Jim Bailey,[1] Edward N. Wright,[2] Xuhua Wang,[1] Alison B. Walker,[2] Donal D. C. Bradley,[1] and Ji-Seon Kim[1,a)]
[1]*Department of Physics and Centre for Plastic Electronics, South Kensington Campus, Imperial College London, London SW7 2AZ, United Kingdom*
[2]*Department of Physics, University of Bath, Bath BA2 7AY, United Kingdom*

(Received 31 March 2014; accepted 13 May 2014; published online 28 May 2014)

Insertion of ultra-thin polymeric interlayers (ILs) between the poly(3,4-ethylenedioxythiophene): polystyrene sulphonate hole injection and poly(9,9-dioctylfluorene-*alt*-benzothiadiazole) (F8BT) light emission layers of polymer light emitting diodes (PLEDs) can significantly increase their efficiency. In this paper, we investigate experimentally a broad range of probable causes of this enhancement with an eye to determining which IL parameters have the most significant effects. The importance of hole injection and electron blocking was studied through varying the IL material (and consequently its electronic energy levels) for both PLED and hole-only diode structures. The role of IL conductivity was examined by introducing a varying level of charge-transfer doping through blending the IL materials with a strong electron-accepting small molecule in concentrations from 1% to 7% by weight. Depositing ILs with thicknesses below the exciton diffusion length of ~15 nm allowed the role of the IL as a physical barrier to exciton quenching to be probed. IL containing PLEDs was also fabricated with Lumation Green Series 1300 (LG 1300) light emission layers. On the other hand, the PLEDs were modeled using a 3D multi-particle Kinetic Monte Carlo simulation coupled with an optical model describing how light is extracted from the PLED. The model describes charge carrier transport and interactions between electrons, holes, singlets, and triplets, with the current density, luminance, and recombination zone (RZ) locations calculated for each PLED. The model shows F8BT PLEDs have a narrow charge RZ adjacent to the anode, while LG 1300 PLEDs have a wide charge RZ that is evenly distributed across the light emitting layer. Varying the light emitting layer from F8BT to Lumation Green Series 1300, we therefore experimentally examine the dependence of the IL function, specifically in regard to anode-side exciton quenching, on the location of the RZ. We found an exponential dependence of F8BT PLED luminance on the difference, δ, in the highest occupied to lowest unoccupied molecular orbital energy gap between the light emitting polymer and a semiconducting polymeric IL, with δ consequently the most important parameter determining efficiency. Understanding the exponential effect that wider energy gap IL materials have on exciton quenching may allow δ to be used to better guide PLED structure design. © *2014 AIP Publishing LLC*. [http://dx.doi.org/10.1063/1.4879455]

I. INTRODUCTION

Light-emitting, vacuum-deposited organic small-molecule LEDs are increasingly being used in commercial displays for mobile phones and televisions. Polymer light emitting diodes (PLEDs) have not yet achieved a corresponding commercialization but impressive demonstrators have been shown and there is a view that their ability to be manufactured using printing methods offers significant cost advantages. In that regard it is worth noting that for lighting applications there is already a consensus that small molecule organic light emitting diodes (OLEDs) will need to be solution processed in order to reach a reasonable price point. Simpler device architectures are also needed to fabricate large area, high efficiency devices. Recent work in hybrid organic-inorganic LEDs (HYLEDs) has realized high luminous efficiencies in an inverted structure with a metal oxide cathode layer.[1–4] Yet the highest luminous efficiencies in such devices are only achieved by replacing the standard ~100 nm thickness light emitting polymer (LEP) layer with a micrometer thick LEP layer, resulting in high operating voltages and consequently low power efficiencies. The inclusion of a 10–15 nm interlayer (IL) of poly(9,9-dioctylfluorene-*co*-N-(4-butylphenyl)-diphenylamine) (TFB) between the poly(3,4-ethylenedioxythiophene):polystyrene sulphonate (PEDOT:PSS) hole injection layer and poly(9,9-dioctylfluorene-*alt*-benzothiadiazole) (F8BT) emission layer significantly enhances performance,[5] also for inverted structures.[6] The dominant mechanism of the efficiency increase has not yet been clearly identified although it has been carefully studied for related PLEDs with poly(9,9-dioctylfluorene-*alt*-bithiophene) (F8T2) light emission layers.[7]

In simple thin-film PLEDs, a transparent indium tin oxide (ITO) anode typically injects holes into the light-emission layer *via* a PEDOT:PSS conducting polymer layer, while electrons are injected *via* a low work function metal cathode. The PEDOT:PSS layer increases the ITO anode

a)Author to whom correspondence should be addressed. Electronic mail: ji-seon.kim@imperial.ac.uk.

work function from ~4.6–4.8 eV to ~5.1–5.2 eV, thereby assisting hole injection.[8] In this structure, the IL is applied on top of the PEDOT:PSS where it forms a physical barrier that improves device performance, probably by both preventing the acidic PEDOT:PSS from degrading the active layer and also by limiting exciton quenching through moving the recombination zone (RZ) away from the ITO anode.[5,7,9] The IL could also improve hole injection, hinder electrons from reaching the anode, and promote a better charge balance within the LEP layer.[7] Previous work in the literature has focused on studying the role of the IL as an electron blocking and/or hole injecting layer[10–12] and in promoting charge balance within the emission layer.[10,13] The IL effect on pinning of the light emission layer's Fermi level to that of the PEDOT:PSS hole injection layer[14] has also been considered.[7] IL conductivity, a parameter that should also have an effect on efficiency, has not been adequately investigated in the literature[10] although the contributing effect of mobility has.[7] There are clearly many parameters to take into account, but no study has investigated them all. This study focuses specifically on investigating the relative effect that the major IL parameters have on the performance of thin-film F8BT PLEDs.

F8BT emission layer PLEDs were fabricated with three different semi-conducting polymer IL materials, two arylamine-fluorene copolymers (TFB and poly(9,9-dioctyl fluorene-co-bis(N,N′-(4,butylphenyl))bis(N,N′-phenyl-1,4-phenylene)diamine) (PFB)) and one bithiophene-fluorene copolymer (poly(9,9-dioctlyfluorene-co-bithiophene) (F8T2)). Their different energy levels (listed alongside their chemical structures in Table I) allow the role of electron blocking and hole injection barriers to be studied. The strong electron acceptor tetrafluoro-tetracyanoquinodimethane (F_4TCNQ) was blended with the IL materials in varying concentrations to p-dope them in order to examine the role of IL conductivity on PLED performance. To investigate whether ILs with thicknesses below the exciton diffusion length (~15 nm)[5,24,25] can prevent luminance quenching by the anode, we spin-coated <5 nm thick layers by using concentrations of <1 mg/ml of the IL materials. F8BT has a relatively deep lowest unoccupied molecular orbital (LUMO) and a reasonably high electron mobility,[21,26] which combined with a relatively deep highest occupied molecular orbital (HOMO) may lead to preferential electron injection and transport and consequently an electron-hole RZ lying adjacent to the anode. Another green emitting active layer, Lumation Green Series 1300 (LG1300, also known as Green K)[1,27,28] was used to study the effect of RZ location on the role of the IL. LG1300 has relatively balanced electron and hole mobilities and should therefore have a broad, centrally located RZ.[29,30] 3D multi-particle Kinetic Monte Carlo (KMC) simulations that include the transport of and

TABLE I Material chemical structures and their electronic energy levels.

Material	Chemical structure	E_a [a,b] (eV)	I_p [b,c] (eV)	E_g [d] (eV)
TFB	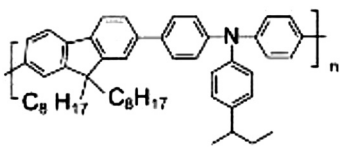	2.3 (Ref. 15)	5.3 (Ref. 16)	3.0
PFB	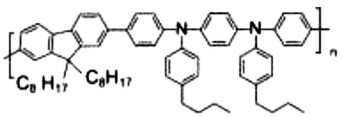	2.3 (Ref. 17)	5.1 (Ref. 16)	2.8
F8T2	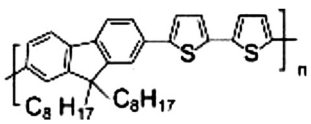	3.2 (Ref. 18)	5.5 (Refs. 18 and 19)	2.3
F_4TCNQ	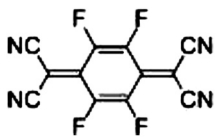	5.24 (Ref. 20)	…	…
F8BT	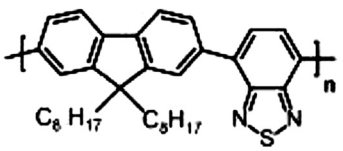	3.3 (Refs. 21 and 22)	5.9 (Refs. 21 and 22)	2.6
LG 1300[e]		2.9 (Ref. 23)	5.4 (Refs. 12 and 23)	2.5

[a] E_a is the electron affinity.
[b] E_a and I_p values are accurate to ±0.1 eV and taken from the literature on the basis of being measured by the same method for comparability.[15,16,18–22]
[c] I_p is the ionization potential.
[d] E_g is the energy gap, I_p–E_a.
[e] LG 1300 is a complex copolymer containing fluorene moieties, arylamine moieties for hole injection, and BT moieties for good electron injection properties. The BT moieties are also responsible for the polymer's green electroluminescence emission. LG 1300 was supplied by the Sumitomo Chemical Company.

interactions between electrons, holes, singlets, and triplets, coupled with an optical model describing how light is extracted from the PLED, have been used to calculate the current density, luminance, and the location of the RZ in both LG 1300 and F8BT PLEDs with and without ILs. KMC modeling offers many benefits over other simulation techniques. The simulation parameters used within KMC are linked to molecular properties unlike the conventional drift diffusion models concerned with average properties across a layer of the device. In addition to this, the KMC model explicitly calculates the coulombic interactions between electrons and holes, making exciton formation, transport, and recombination possible to model, something which is typically lacking in the approach of finding steady state solutions to the 3D Pauli master equation.

Here, we demonstrate the importance of preventing exciton quenching at the anode and cathode sides of the light emitting layer. Small changes in the energy gap differences of the LEP and adjacent organic layers can have a large effect on the luminance, especially when the RZ lies adjacent to the interface. Based on the results of our study, we propose that ILs with wider energy gaps could lead to the design of more power efficient PLEDs while retaining a thin-film device structure.

II. EXPERIMENTAL METHODS

PLED structures, as detailed in Fig. 1, were fabricated by first spin-coating a 35 nm layer of PEDOT:PSS (Baytron P VP AI4083) onto ITO-coated glass substrates and then thermally annealing this layer at 135 °C for 30 min. For those devices without an IL, a 60 nm layer of F8BT (or 70 nm layer of LG 1300) was then spin-coated on top of the PEDOT:PSS from a toluene (or chlorobenzene) solution. These devices were then completed by thermally depositing 20 nm of Ca capped by 140 nm of Al. Each pixel, as defined by the spatial overlap of the anode and cathode, had an area of 4.5 mm^2. The IL devices were fabricated in the same way, except that a 10–15 nm TFB (or PFB) or 2–5 nm F8T2 layer was deposited on top of the PEDOT:PSS from toluene solution and thermally annealed at 180 °C for 60 min prior to spin-coating F8BT (or LG 1300).[5] The annealing step helps to prevent the IL material being washed away or intermixing with the emission layer material when the latter is deposited on top from organic solvent solution.[5] These IL thicknesses represent the thickest insoluble layers of each material that could be formed *via* thermal annealing. Thinner ILs were created by spin-coating from more dilute solutions. Doped ILs were spin-coated from toluene solutions of the IL material blended with 1%, 3%, or 7% F_4TCNQ by weight. For hole-only diode structures, the Ca/Al top contact was replaced with Au, which has a high work-function. Current-voltage (J-V) characterization of the PLEDs and hole-only devices was carried out in a nitrogen atmosphere test chamber using a computer-interfaced Keithley 2400 SourceMeter. PLED luminance was measured with a Minolta LS100 luminance meter and electroluminescence (EL) spectra with an Ocean Optics USB 2000 CCD spectrophotometer.

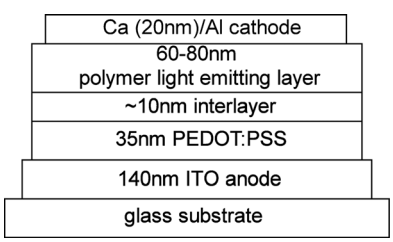

FIG. 1. Schematic PLED device structure used for our experiments. F8BT and LG 1300 were used for the light emitting polymer layer. TFB, PFB, and F8T2 were used as IL materials. In addition, some devices were fabricated without ILs. Hole-only device structures used Au as top contact instead of Ca/Al.

UV-visible absorption and photoluminescence (PL) spectroscopy measurements of the PEDOT:PSS/IL component of the device stack were performed on samples deposited on quartz substrates. For ultraviolet photoelectron spectroscopy (UPS) measurements, the same structure was used, but with glass/ITO as the substrate instead of quartz. The effect of annealing was studied for both doped and undoped IL samples by measuring their PL behavior before and after the annealing step. The measurements were carried out for samples held within an integrating sphere using scattered laser light to excite them. PL studies were carried out using a Jobin-Yvon Fluoromax spectrofluorometer. Excitation wavelengths were selected to lie close to the respective absorption maxima, namely, 380 nm for TFB and PFB, and 360 nm for F8T2. The samples were placed inside an integrating sphere, again offset from direct illumination by the excitation beam. The doped and undoped IL series were annealed prior to UPS measurements. They were excited with a He I, 21.2 eV beam, with an Au electrode as reference. Raman measurements were carried out on films drop-cast or spin-coated onto quartz substrates, using 633 nm laser excitation.

III. SIMULATION METHODS

The results of simulations performed using a combined multi-particle 3D KMC and optical model were compared to the experimental PLED data. The electronic and optical processes were calculated within the simulation for voxels placed on a regularly spaced user designed 3D Cartesian lattice of lattice constant $a = 1.0$ nm, a typical value used in Monte Carlo simulations[31–33] and a good approximation to the physical volume of a monomer unit. Each voxel represented a hopping site available to electrons, holes, singlets, or triplets with certain parameters describing separately how each of these species interacts with the material the voxel is representing (F8BT, PFB, TFB, or F8T2). Periodic boundary conditions were always applied in the y and z dimensions, with electrodes at $x = 0$ and $x = LX$, where LX denoted the thickness of the device. The electrodes were assumed parallel to the (y,z) plane. Bipolar charge injection and extraction through electrodes were governed by the conventional Miller-Abrahams rate equation,[21–24] and charge transport through the bulk of the device was governed by a Marcus-theory-derived hopping process between voxels,[31,34] where the energy of each site was randomly selected from a Gaussian distribution of width σ, centered on the HOMO

and LUMO level of each polymer material.[35] The Marcus hopping rate was proportional to a material dependent mobility fitting parameter, μ_{iso}, which represented the high temperature limit of carrier mobility within the material. Charges within the device electrically interacted with each other and their induced image charges, and charges of opposite polarity could combine to form either singlets or triplets. Diffusion of singlets was described using the Förster energy-transfer rate,[36] which was considered a good representation of singlet diffusion in our coarse grained model, which did not distinguish between intra- and inter-chain hopping processes.

$$R_E = \frac{1}{\tau_s} \times \left(\frac{r_F}{d_j}\right)^6 \times e^{-\left(\frac{E_i - E_j}{k_B T}\right)}, \quad (1)$$

where R_E is the exciton diffusion rate and τ_s is the singlet lifetime. The term E_i–E_j represents the change in the energy between the initial site, i, and destination site, j; when the initial and destination sites are located on polymer chains of different materials the term is equivalent to the difference in energy gaps of the two materials. The second term of the equation describes the effect that the distance between donor and acceptor sites affects the rate, with the sixth power term originating from a point-to-point dipole-dipole interaction; r_F is the Förster radius. F8BT has an experimentally determined singlet diffusion length of approximately 15 nm,[5,24,25] so a value of 10.5 nm for the Forster radius was chosen, since this gave a simulated singlet diffusion length of 15 nm. The distance between donor and acceptor is d_j. This approximation does not obviously hold for polymer chains in which the excited state can be extended over distances comparable to or larger than the chain-chain separation distance; weaker power dependences would then apply.[38] For simplicity, however, we have assumed here that the point-to-point dipole-dipole interaction description suffices to first approximation. Triplet diffusion was governed by Dexter energy transfer which was approximated by a Miller-Abrahams type hopping between nearest neighbors.[37]

Singlets and triplets are assumed to be generated in a 1:3 ratio due to spin statistics, where interaction between singlets and triplets are governed by the pathways described by Zhang and Forrest.[39] The recombination and dissociation of singlets and triplets are modelled with respective rates dependent on the material and include triplet-triplet annihilation reactions that can cause a higher than 25% yield of singlets, as modelled in Ref. 39.

The core of the model works as follows: if each event (hole hop, singlet recombination, etc.), i, has an associated rate, k_i, then the time, t_i, it takes for the event to occur is calculated by

$$t_i = -\ln(R_i)/k_i, \quad (2)$$

where R_i is a uniformly distributed random number between 0 and 1. The simulation proceeds by calculating all available events and then executing the event with the lowest time, t_i, associated with it. Once the fastest event has been executed all possible events in the system are recalculated based on the new state of the system, and the simulation clock changes by $t_{sim} + t_i$. An optical model exploiting the equivalence between an oscillating dipole antenna in a non-absorbing medium and the probability of a recombinative dipole transition in thin-film microcavities has been used to calculate the outcoupling probability, $E_{out}(x)$, of a photon escaping the device once generated by the radiative recombination of a singlet. Further details of the model can be found in the literature.[40] The optical model is also used to adjust the radiative decay rate of singlet excitons due to the microcavity. Luminance, L, and current density, J, measurements can be compared with our combined electrical and optical simulations. The current density is the flow of charge per unit area that has passed through the electrodes, and the luminance is calculated as[41]

$$L = \left(\frac{1}{\pi}\right) h\nu k_m \int_0^x E_{out}(x) S(x) dx, \quad (3)$$

where k_m is the maximum spectral efficiency defined by the International Commission on Illumination and is equal to 683 lm W^{-1}. The simulation assumes a monochromatic emitting green PLED of wavelength $\lambda = 560$ nm. $S(x)$, calculated directly from the KMC model, is the singlet recombination profile and is given as the positional likelihood that photons will be generated within the device per unit area.

IV. RESULTS

A. Varying the interlayer material

Fig. 2 shows current density-voltage (J-V (a)), luminance-voltage (L-V (a)), cd A^{-1} (c) and lm W^{-1} (d) efficiency, and EL spectra (e) for the F8BT PLEDs with and without ILs. The J-V data for hole-only (ITO/PEDOT:PSS/IL/F8BT/Au) devices with the same IL series are also shown in (b). The EL spectra for the PLEDs with ILs have a reduced full-width-at-half-maximum (FWHM) linewidth relative to the IL-free device, with a loss of intensity from the long wavelength side of the peak. As this change is observed with all ILs, we propose that these changes in EL emission are caused by a difference in the packing of the F8BT polymer chains[42] that occurs when F8BT is spincoated onto a hydrophobic surface, compared to the hydrophilic surface of the PEDOT:PSS layer. In the literature, a strong PL emission peak at ~625 nm is found in PFB:F8BT blends due to exciplex states at the PFB:F8BT heterojunction.[43–45] No clear exciplex features are visible at low energies although there is a slight increase in deep-red emission from the PLED with a PFB IL, which indicates that some exciplex emission may be present in that device.

Below turn-on, the J-V curves are symmetric at low bias voltages (below 1.5–2.0 V) which indicate that there is a small number of shunt paths between the anode and cathode causing short circuit currents.[27,46] PLEDs with F8T2 ILs display currents in this regime that are an order of magnitude higher than in the other PLEDs, implying increased shorting. The current threshold (where conduction through the semiconductor becomes more important than the short circuit currents) varies with the IL material used (1.50 V for PFB,

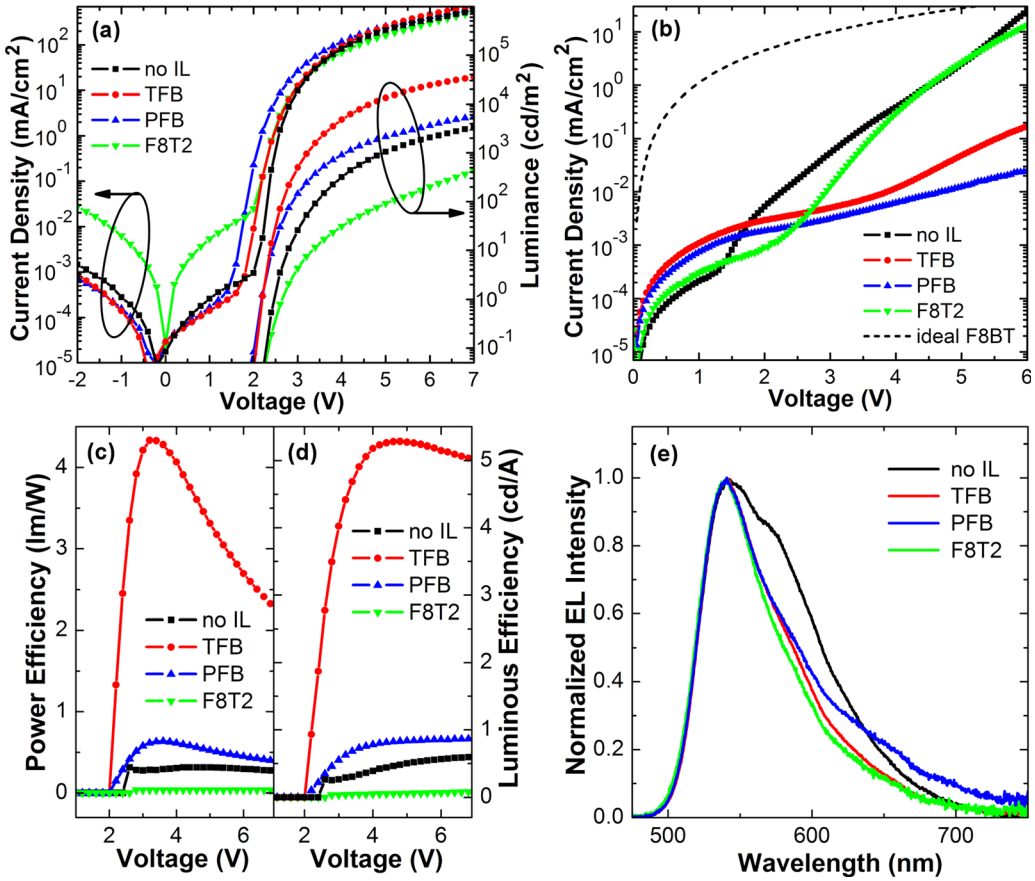

FIG. 2. (a) *J-V* and *L-V* curves for F8BT PLEDs with and without ILs; (b) *J-V* curves for hole-only ITO/PEDOT:PSS/IL/F8BT/Au devices and the estimated SCLC density of an F8BT PLED without an IL (see text for details). Efficiencies derived from the curves in (a) are presented in (c) lm W^{-1} and (d) cd A^{-1}. The PLED EL spectra are shown in (e).

1.74 V for TFB, 1.96 V for F8T2, and 2.11 V without an IL with an error of ±0.15 V). These values were obtained from the intersection of straight line extrapolations of the *J-V* curves around the current turn-on. The trend in the threshold values corresponds clearly with the increasing energy injection barriers between the IL materials (or PEDOT:PSS when no IL was used) and F8BT (see Table I).

The high current density regime above 100 mA cm^{-2} in Fig. 2(a) is relatively unaffected by changing the IL material, in contrast to the luminance, which varies by around two orders of magnitude in the same voltage range. Compared to the IL-free PLED, inclusion of a F8T2 IL causes a drop in luminance, while use of a PFB IL raises it, with the highest luminance for a TFB IL. The maximum power efficiencies of the devices correlate with their maximum luminance values. TFB IL devices achieved 4.33 lm W^{-1} at 3.2 V, whilst PFB devices reached 0.43 lm W^{-1} at 2.8 V. F8T2 IL devices meanwhile showed a maximum efficiency of 0.04 lm W^{-1} at 7.2 V, lower than the devices without an IL which gave 0.31 lm W^{-1} at 4.8 V. The F8T2 IL device performance also lags that of F8T2 PLEDs in which a 60 nm F8T2 film was used as the emission layer, sandwiched between 50 nm of PEDOT:PSS (Clevios P AI4083) and a 20 nm Ba/100 nm Al bilayer cathode.[18] In this latter case, a maximum 2 lm W^{-1} efficiency was achieved, falling to 1.2 lm W^{-1} at 1000 cd m^{-2}.

Both TFB and PFB display a relatively large (1.0 ± 0.1 eV) electron blocking LUMO offset relative to F8BT, yet PFB IL devices perform considerably worse than TFB IL ones. This suggests that electron blocking might not be the primary cause of efficiency increases. F8T2 IL PLEDs have only a negligible barrier for electron blocking such that TFB has previously been used as an IL when F8T2 is used as emission layer.[7]

If reduction of the hole-injection barrier were the crucial factor, we would expect PFB IL devices to be the most efficient but they are not. Furthermore, the lowered luminance of F8T2 IL devices—where the hole-injection barrier is reduced relative to IL-free devices—also implies that hole-injection barriers alone are not the dominant factor in achieving the highest efficiencies in the F8BT PLED system studied here.

The hole-only devices were fabricated with Au contacts to block electrons from being injected. At high bias voltages, such a contact may not provide sufficient electron blocking, so only the data up to 6 V are shown. For comparison, the ideal trap-free current density as calculated using the space charge limited current (SCLC) equation[47] for an F8BT PLED without an IL is illustrated with a dashed line in Fig. 2(b). A hole mobility of 8×10^{-7} cm^2 V^{-1} s^{-1} was used in the calculation, which had been determined through hole-only device measurements on the same batch of F8BT polymer as used in this experiment.[48] The SCLC equation thus provides the maximum possible current density that would be achievable in our devices if they were trap-free and

had perfect, i.e., ohmic, charge injection. The *J-V* characteristics of the hole-only devices in Fig. 2(b) show that the hole currents observed in all our devices fall short of the ideal situation: lower overall current densities imply that hole traps reduce hole transport, while the various regimes visible in the shape of the curve indicate a field dependent hole mobility.

Fig. 2(b) further shows that for significant (i.e., $>10^{-2}$ mA cm^{-2}) hole-injection to occur from the ITO/PEDOT:PSS/IL stack into F8BT, higher voltages are required than when the IL is absent. This is in contrast to the trend in the threshold voltages in the bipolar devices and indicates that electron build-up at the interface plays a non-trivial role in PLED hole-injection. The current densities achieved above turn-on are lower by more than an order of magnitude in devices using TFB and PFB ILs. However, as the hole currents in a F8BT PLED make up a small percentage of the overall current density, due to the electron mobility of F8BT being substantially higher than the hole mobility,[21,22] this observation is not in contradiction to the results from the bipolar devices, which did not show significant variations in *J* between the various IL devices. Interestingly, the results indicate that the triarylamine containing ILs decrease the hole-only diode stack's hole transporting abilities, compared to the dithophene containing IL, although the triarylamine ILs both have lower hole injection barriers to PEDOT:PSS. The hole mobilities for TFB,[49,50] PFB,[49] F8T2,[26] and F8BT[51] recorded in the literature vary significantly not only between the materials but also for the same materials; they are, however, generally within the same order of magnitude ($\sim 10^{-3}$ cm^2 V^{-1} s^{-1}). The larger hole currents in the F8T2 IL hole-only devices do not translate into higher efficiencies in the PLEDs.

To summarize, we have shown that in our IL devices electron blocking does not play a dominant role in achieving the highest device efficiencies. Luminance changes do not correlate with the hole injection barriers in bipolar devices or with the current densities of hole-only devices. Hole injection and electron blocking effects therefore seem not to play a major role in the function of the ILs.

B. Doping the interlayer

Previous research has shown that F_4TCNQ is a good p-dopant of organic semiconductors[52] and enhancement of the conductivity of both TFB and PFB *via* F_4TCNQ doping.[20] Fig. 3 shows 633 nm excited Raman spectra for F8T2, F_4TCNQ, and a drop-cast film deposited from a solution of F8T2 blended with 15% w/w F_4TCNQ. A vibrational peak appears at 1370 cm^{-1} in the Raman spectrum of the F_4TCNQ doped F8T2 film that is not present in either of the other two spectra. This peak originates from the charged F_4TCNQ^- dopant molecule adopting a non-planar conformation.[53] In addition, the strong background fluorescence (rising from left to right in the F8T2 Raman spectrum) associated with the F8T2 PL peak[18] is absent in the doped film. This is consistent with the formation of exciton-quenching charged polaron/bipolaron states within

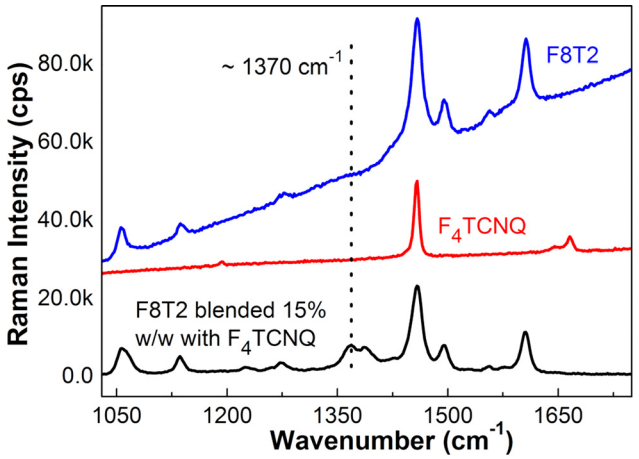

FIG. 3. Raman spectra of (from bottom to top) a drop-cast blend film of F8T2 with 15% w/w F_4TCNQ, and neat F_4TCNQ and F8T2 films. The PL background evident in the latter is quenched for the 15% doped F8T2 sample.

the HOMO-LUMO energy gap[54] and therefore confirms that F8T2 is oxidatively doped with F_4TCNQ.

Figs. 4(a)–4(c) show the *L-V*, *J-V*, and power efficiency *vs.* voltage curves of F8BT PLEDs with TFB, PFB, and F8T2 ILs, respectively. F8T2 IL PLEDs with doped ILs had higher leakage and reverse bias currents than the reference IL-free PLED, which can be explained by increases in conduction *via* shunt paths. In contrast, the leakage currents for devices with doped PFB and TFB ILs are of the same order of magnitude as that of the reference IL-free device. The absence of an increase in the reverse bias currents in TFB and PFB IL PLEDs indicates clearly that no doping of the adjacent F8BT layer is occurring. The current and luminance turn-on voltages are unaffected by doping as far as can be determined (within ~0.5 V). After current density turn-on neither the luminance nor the current density curves are significantly affected by the addition of more dopant. The PLEDs containing ILs with 7% F_4TCNQ dopant achieved maximum power efficiencies of 2.02 lm W^{-1} at 4.4 V for TFB, 0.43 lm W^{-1} at 3.8 V for PFB, and 0.05 lm W^{-1} at 4.0 V for F8T2. In all cases, only minor differences in current density are recorded after *J* turn-on for doped and undoped ILs. Luminance values are also minimally affected.

The EL spectrum of IL-free F8BT PLEDs (Fig. 4(d), dashed line) displays a strong peak centered on 545 nm with a broad shoulder at around 575 nm. The EL spectra for PLEDs with 7% F_4TCNQ doped TFB and F8T2 ILs have the same spectral characteristics as each other—with a slight increase in shoulder/red-edge emission relative to the IL-free device. The 7% F_4TCNQ doped PFB IL device is somewhat different, with a significant increase in long wavelength EL emission. In contrast to the situation for the undoped-IL PLEDs (c.f., Fig. 2(e)), doped-IL devices have a higher proportion of the long wavelength (575 nm) shoulder EL. We propose the changes may be due to the dopant molecules changing the IL surface, leading to a different packing of the F8BT polymer chains, which may cause changes in EL emission[42] or due to exciplex emission from F8BT:F_4TCNQ.

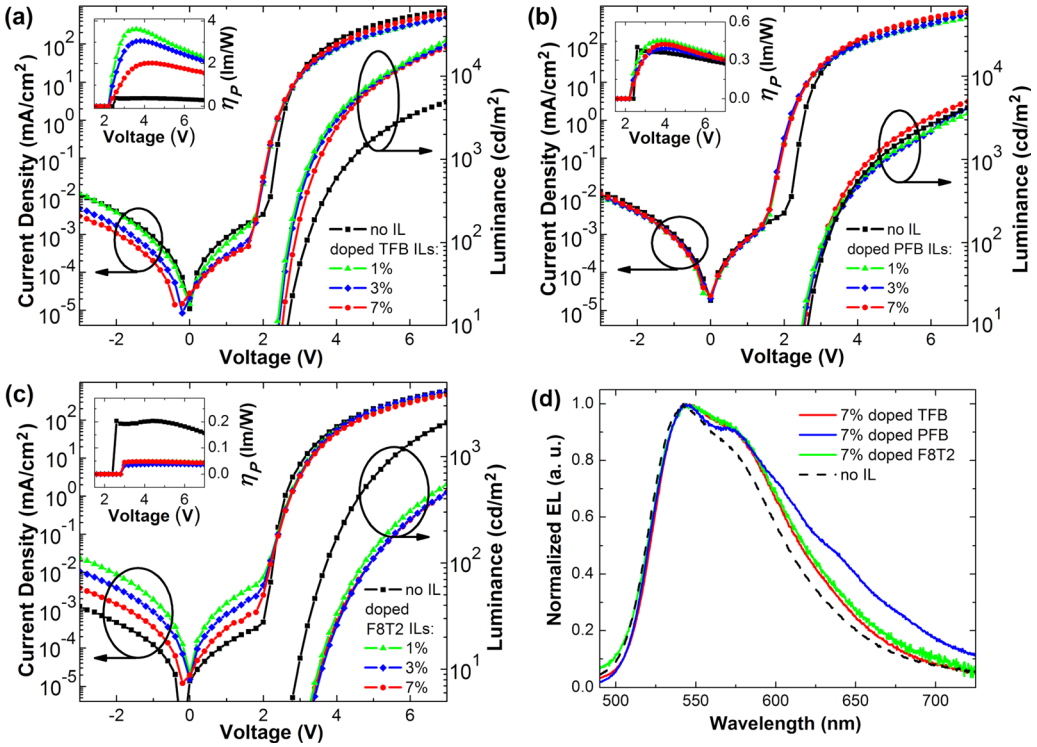

FIG. 4. *J-V* and *L-V* data for F8BT PLEDs with 1%–7% by weight F_4TCNQ doped (a) TFB, (b) PFB, and (c) F8T2 ILs. IL-free reference devices were also fabricated for each IL series and the corresponding data are shown in each panel. EL spectra recorded at 5 V for the 7% F_4TCNQ doped-IL and IL-free devices are shown in (d).

Fig. 5 shows *J-V* data from hole-only devices with 7% F_4TCNQ doped ILs and for a reference device without an IL. The voltages at which the hole-only devices turn-on did not change appreciably upon doping the ILs, consequently the data for the undoped ILs is not shown. Doping slightly decreases current density in hole-only diodes with F8T2 ILs. When a doped PFB IL is used the current density below 4 V is lower compared to device with an undoped PFB IL by around an order of magnitude; above 4 V, the current density approximately matches that of the undoped PFB IL device. With a TFB IL the current density in the hole-only diode structure is reduced consistently by around an order of magnitude. The decrease in the hole-only diode current when adding dopant to the TFB IL is significant; however, the decreases in current are larger compared to differences between a TFB IL and an IL-free hole-only devices—in the latter case the efficiency is significantly increased, while it is slightly decreased in the former case. This implies that the current densities of the hole-only devices are a poor predictor of PLED efficiencies.

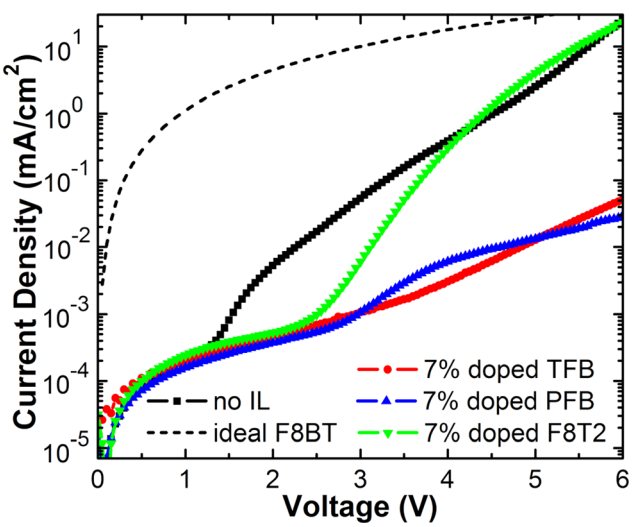

FIG. 5. Current density *vs* voltage data for Au-cathode, hole-only devices with 7% F_4TCNQ doped ILs and for a reference device without an IL. The estimated SCLC density of an F8BT PLED without an IL is indicated with a dashed line (see text for details).

Additionally, UPS measurements were carried out on ITO/PEDOT:PSS/IL samples with and without addition of 1%, 3%, and 7% F_4TCNQ dopant. The ionization potential (I_p) of F8T2 was measured as 5.5 ± 0.1 eV, which is in good agreement with the literature value of 5.5 eV listed in Table I, thus confirming that the electronic states of the F8T2 IL film are being probed. The doped ILs show smaller I_p values that should decrease the hole injection barrier from PEDOT:PSS coated ITO electrodes (workfunction $= 5.2 \pm 0.1$ eV). The I_p values of the TFB and PFB ILs are within 0.5 eV and 1.0 eV of commonly cited literature values. Doping the PFB and F8T2 ILs decreases their I_p values while this effect is only visible for the lowest dopant concentration in TFB, with higher dopant concentrations returning I_p to its undoped value. In all three cases, the 1% dopant concentration has the biggest effect on I_p, with higher dopant concentrations showing a lesser, if any, effect—this implies only small concentrations of the dopant are required for doping saturation to be achieved.

To summarize, both PLED current density and luminance vary minimally with IL doping level. There was similarly no

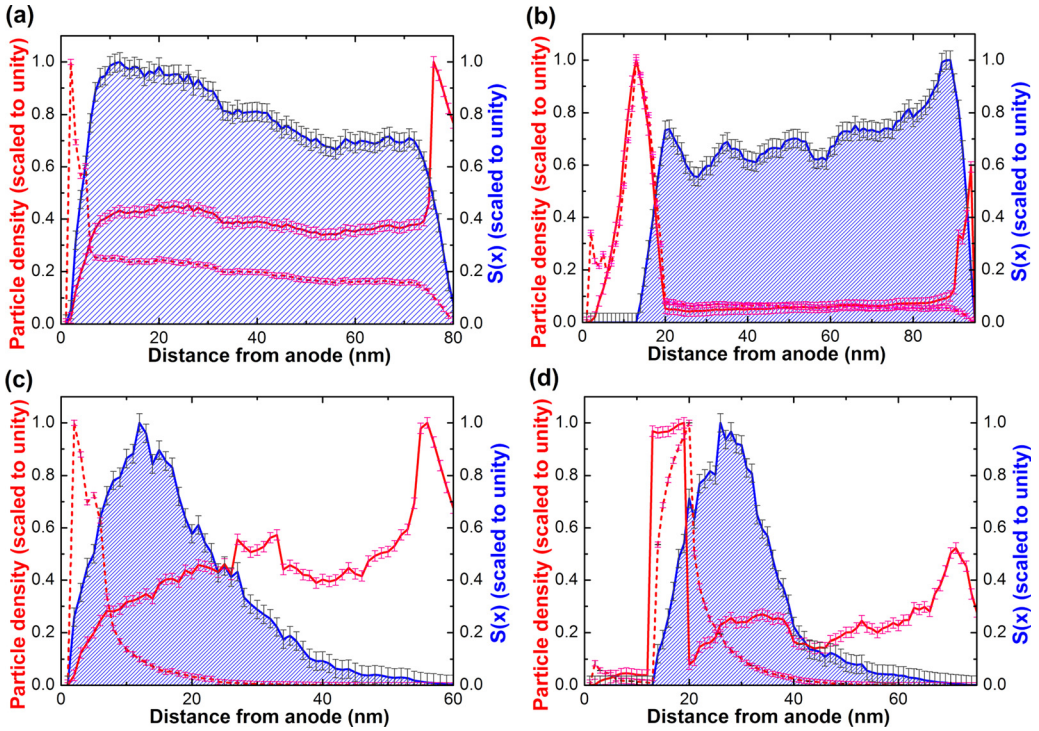

FIG. 6. Device simulations at 5.2 V bias of the hole (dashed) and electron (solid) densities scaled to unity, and the singlet recombination zones, S(x) (shaded), for a LG 1300 PLED (a) without an IL (cathode located at 80 nm from the anode) and (b) with a TFB IL (cathode located at 95 nm from the anode). Data are also shown for a F8BT PLED (c) without an IL (cathode located at 60 nm from the anode) and (d) with a TFB IL (cathode located at 75 nm from the anode).

clear correlation between PLED efficiencies and current densities in corresponding hole-only diode structures. In addition, decreased I_p values were deduced from the UPS spectra.

C. Varying the emissive layer material

Fig. 6 shows the KMC model predicted electron (solid line) and hole (dashed line) profiles for F8BT and LG 1300 devices with and without ILs. The electron and hole profiles are calculated by taking snapshots of particle locations once the model has reached a steady state. Also shown is the recombination zone of singlets, *S(x)*, (shaded area), is calculated in a similar manner as Staudigel *et al.*[41] by recording the locations of all singlet recombination events. The anode is located at x = 0 nm. These data suggest that for LG 1300 PLEDs the RZ is more evenly distributed across the active layer of the device, while that for F8BT PLEDs the RZ is localized on the anode side.

This is reasonable on the basis that the conjugated backbone of LG 1300 contains fractions of arylamine, benzothiadiazole (BT), and fluorene moieties within a chain architecture that allows for balanced electron and hole mobilities.[55] Trivially, for both F8BT and LG 1300 PLEDs, the RZ is moved away from the anode by the thickness of the added IL but in LG 1300 PLEDs there is also a significant increase in recombination near the cathode and a sharper peaking in the recombination at the anode side of the device. While this relocation of the RZ away from the anode is the main change when inserting the IL, the hole current density profile within the active layer is also significantly affected by the IL. In both F8BT and LG 1300 PLEDs without an IL, the electron densities peak near the cathode side and drop towards zero near the anode side of the devices. In both types of PLEDs, the TFB IL causes the maximum of the electron density to shift from the cathode to the anode side of the devices, with a smaller, but still significant peak in electron-densities remaining near the cathode, which indicates electron-blocking at the anode-side.

The *J-V* and *L-V* curves of LG 1300 PLEDs with and without ILs and their corresponding efficiencies in cd A^{-1} and in lm W^{-1} are shown in Figs. 7(a)–7(c), respectively. The introduction of ILs in this system somewhat reduces the above turn-on current density (Fig. 7(a), left ordinate) for all ILs. As the IL is applied to the anode-side of the PLEDs (c.f., Fig. 6) it is likely that this effect is predominantly the consequence of a reduction in hole current density. More widely varying luminance values are observed (Fig. 7(a), right ordinate), however. The addition of the PFB and F8T2 ILs causes reductions in the luminance (most significantly with the PFB IL). A TFB IL causes a reduction in luminance at low voltages, but a slight increase in luminance at voltages over 5 V. This suggests that the ILs must also cause changes in exciton quenching and/or in the balance of electron and hole densities within the active layer. Efficiency increases are seen above 3.5 V when using a TFB IL and above 6.1 V when using a F8T2 IL (Figs. 7(b) and 7(c)). Fig. 7(d) shows the EL spectra of the LG 1300 PLEDs with and without ILs. In each case, the main EL peak arises at ~541 nm with a more or less prominent shoulder at longer wavelengths. According to[56]

$$E_x = IP_D - EA_A - C, \tag{4}$$

where E_x is the energy of an exciplex state, IP_D the donor ionization potential, EA_A the acceptor electron affinity,

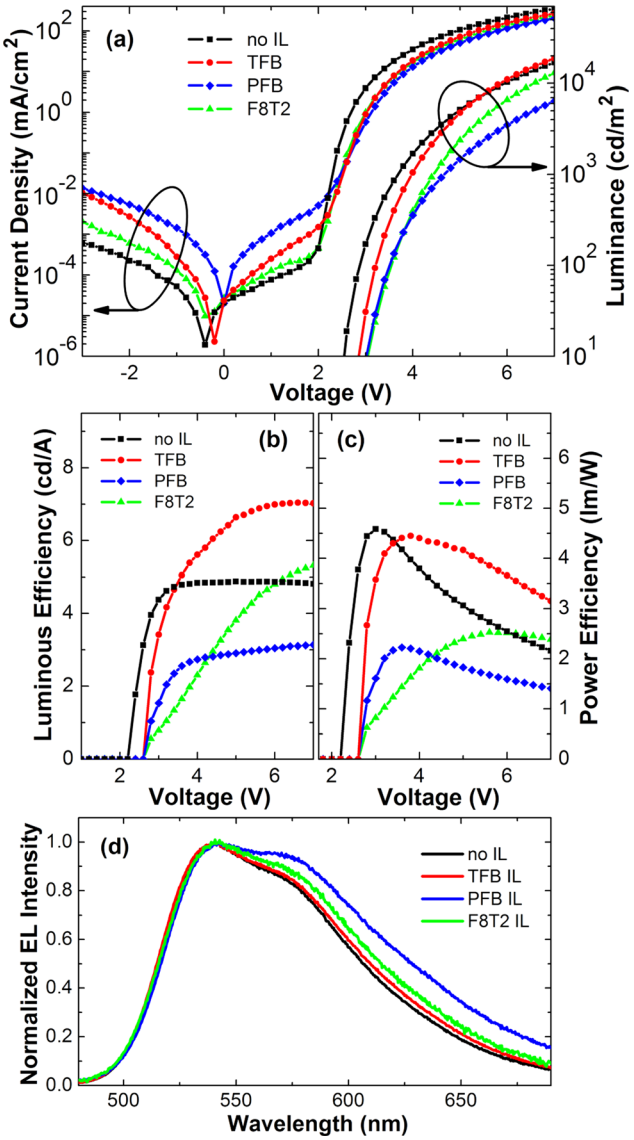

FIG. 7. (a) *J-V* and *L-V*, (b) luminous efficiency, and (c) luminous power efficiency curves, and (d) EL spectra of TFB, PFB, and F8T2 IL PLEDs with a LG 1300 active layer.

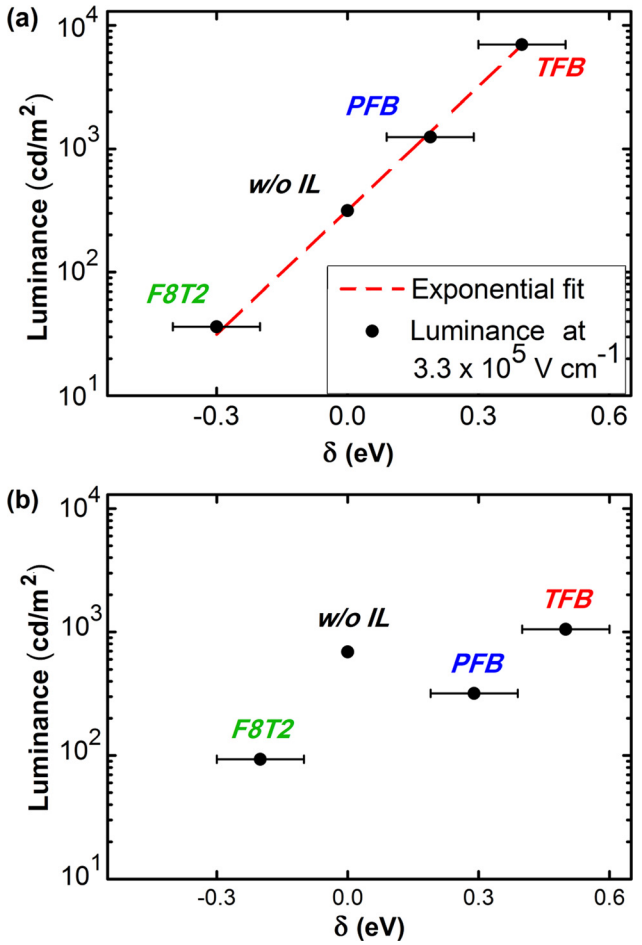

FIG. 8. Luminance recorded at 3.3×10^5 V cm^{-1} (corresponding to voltages near the efficiency maximum of the PLEDs (*ca.* 2.5 V)) for (a) F8BT and (b) LG 1300 PLEDs without an IL and with TFB, PFB, and F8T2 ILs, plotted as a function of δ, the difference in energy between the energy gaps of the IL and emission layer materials. The without interlayer device data are placed at $\delta = 0$ for convenience.

and C the Coulomb stabilization energy associated with the charge-transfer interaction, the LG 1300:PFB exciplex emission would be expected to appear around 600 ± 30 nm (Table I gives a PFB HOMO to LG 1300 LUMO gap of 2.2 eV and C is assumed to be 0.15 ± 0.10 eV).[56] A peak attributable to such emission is centred at 620 nm when the spectrum of the IL-free device is subtracted from the PFB IL device.

Figs. 8(a) and 8(b) show the luminance values of the F8BT and LG 1300 PLEDs, respectively, plotted against δ, the energy gap difference (in eV) between the emission and IL materials. The error in δ was estimated in each case from the associated uncertainties in the gap energies. Though no clear correlation between the luminance and δ is observed in the LG 1300 IL PLED series, the results from the F8BT PLEDs showed an exponential dependence of the luminance on δ, fitted according to

$$L(\delta) = L_0 \times e^{\delta/b}, \tag{5}$$

where $L(\delta)$ is the luminance at a specified electric field as a function of δ and $L(\delta = 0) = L_0$ represents the luminance of an IL-free PLED. The parameter b represents the energy required for L to increase by one factor of e. Exponential curves were fitted to the luminance values at various electric field strengths between 3.3×10^5 and 8.0×10^5 V cm^{-1} yielding an average value $b = 0.15 \pm 0.02$. The field strengths roughly cover the entire voltage range from 2.0 V to 7.0 V and an exponential dependence on the luminance was observed within this range. This exponential dependence of the luminance on δ provides evidence that in F8BT devices—in which the majority of excitons will be within a diffusion length of the IL—exciton quenching processes at that interface are of primary importance for PLED performance.[5] It should be expected that $L(\delta)$ will saturate at large enough values of δ, when the overwhelming majority of excitons are blocked from entering the IL. At type II heterojunctions, a low energy exciplex state can be formed in which the exciton is delocalized across two molecules of differing materials. This exciplex state can then be used to split the exciton into holes and electrons in solar cells. Since F8BT has a lower HOMO level than the IL materials used in this study, the electron-hole pair would have its electron

located on an F8BT molecule and its hole located on a molecule of the IL material. Therefore, dissociation is energetically unfavorable, since the electrons would have to move towards the cathode and holes towards the anode. This is also the case when TFB and PFB ILs are used with LG 1300 LEP layers. LG 1300 and F8T2, however, form a type II heterojunction in which exciton dissociation is energetically favorable— these devices nonetheless outperform PFB IL devices, which implies that exciton dissociation at the interface is not a primary factor in determining the efficiency in the set of PLEDs.

Fig. 9(a) shows good fits to the luminance for the F8BT PLEDs (with and without ILs) have been achieved with the 3D KMC simulation. In these simulations, the singlet diffusion length was assumed to be 15 nm, and therefore any singlets that entered the IL were considered to be immediately quenched; this is justified by noting that the emission profile for each PLED device showed no emission from their respective ILs. The transport of excitons across the interface between F8BT and the IL is dependent on the energy gap offset δ which is accounted for in the $E_i - E_j$ term in Eq. (1). The $E_i - E_j$ terms can be thought of as a Boltzman penalty for hops that are unfavorable in energy and acts to restrict the diffusion of excitons into an IL with a wider energy gap or to restrict the diffusion of excitons in the IL back into the active layer, if the active layer has a larger gap. In Fig. 9(b), luminance values from simulations of the F8BT IL PLED series run at 8 V are plotted against δ. We simulated two cases: (i) all excitons that diffuse from F8BT into the IL or to the anode are considered non-radiative (solid line, filled symbols) and (ii) the IL does not quench excitons (dashed line, open symbols). The lower value of δ, the more significant the change in luminance between (i) and (ii). It is clear that when the energy gap offset favors exciton diffusion into the interlayer (as is the case for F8T2) there is a significant difference between the quenched and unquenched luminance. However, as the energy gap offset becomes unfavorable to exciton diffusion, this difference between quenched and unquenched luminance decreases.

We used our model to determine whether the difference in the energy gap between the IL and F8BT alone was accountable for the exponential dependence we observed. We modelled PLEDs with ILs that had a difference in energy gap of $\delta = -0.30$ eV to F8BT (equivalent to using a F8T2 IL), $\delta = 0.19$ eV (equivalent to using a PFB IL), and $\delta = 0.40$ eV (equivalent to using a TFB IL). Excitons at the interface moved into the IL or stayed within the light emitting layer according to the resulting probabilities based on the energy gap difference. In our model, electron and hole movements are determined by the LUMO and HOMO levels, the resulting injection barriers, and the hopping constants. These can be set independently from the energy gap difference. The results in Fig. 9(c) show the modelled luminance values for set values of δ, where the properties that determine electron and hole movement (electron and hole mobility as well as electron and hole injection barriers) have been artificially set to those of F8T2, PFB, and TFB at each of the three values of δ we probed. The results demonstrate that quenching effects due to the energy gap offset in the simulation (shown in Fig. 9(b)) had a far larger effect on the luminance than varying the other parameters. For the case $\delta = -0.3$ eV, higher luminance values are recorded when using the parameters for TFB and PFB compared to using those for F8T2; the luminance values are none the less still lower than for cases with higher δ values with F8T2 parameters.

To conclude this section, an exponential dependence of the luminance seen in the experimental results of the F8BT devices is reproduced by the 3D KCM simulation, and variation of the simulation parameters demonstrated that the most important factor is exciton quenching. This is likely due to the RZ being located close to the anode interface, since an exponential dependence of the luminance on δ is observed in this system, but not in the LG 1300 PLED IL series for which the RZ spreads across the device.

D. Varying the interlayer thickness

The *J-V* curves in Fig. 10 show no noteworthy change in current density between the thick (~5 nm for F8T2 and ~10–15 nm for TFB and PFB) and the thin (~2 nm for F8T2 and ~5 nm for TFB and PFB) ILs. For TFB, however, a drop in luminance is visible when the <5 nm IL is used rather than the <15 nm TFB IL. Assuming that the exciton diffusion length in alternating fluorene-based copolymers is ~15nm,[5,24,25] the drop in luminance with a TFB layer

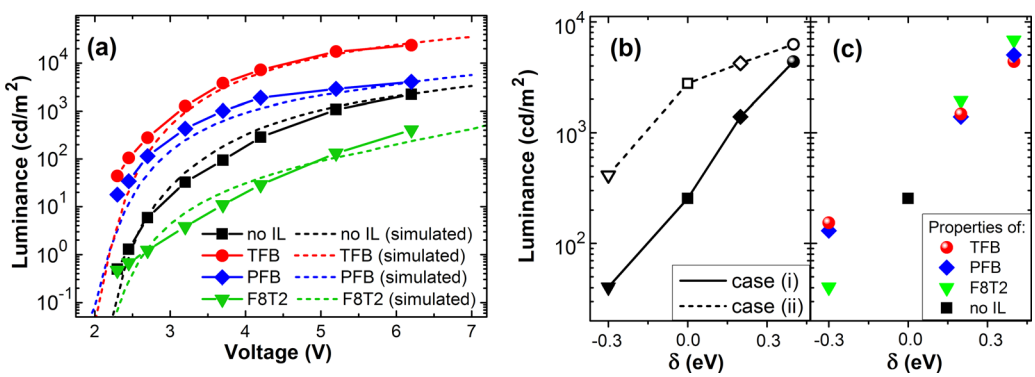

FIG. 9. (a) Comparing the experimental (solid lines) and simulated (dashed lines) luminance of an F8BT light emitting layer PLED with various ILs. (b) How the luminance is affected by quenching due to δ for case (i) with quenching, case (ii) without quenching, and (c) depending on other IL parameters (see text for details).

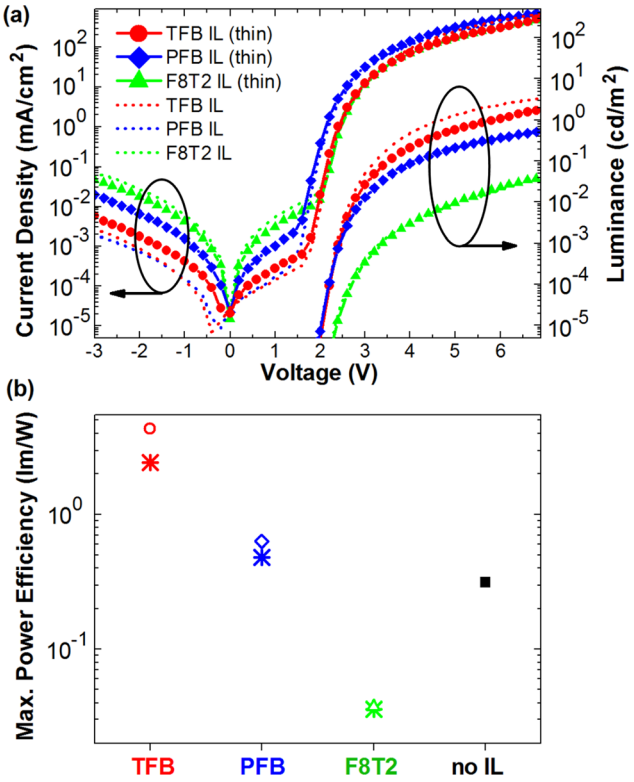

FIG. 10. (a) *J-V* and *L-V* curves of F8BT PLEDs with <15 nm (dotted lines) and <5 nm (solid lines, filled symbols) TFB, PFB, and F8T2 ILs. (b) Maximum power efficiency values on a log scale for an IL-free device and for <15 nm (open symbols) and <5 nm (star symbols) TFB, F8T2, and PFB IL devices.

<5 nm can be explained through the RZ being located closer to the anode, thus increasing luminance quenching. The overall trend in the device efficiencies with various IL materials is not altered by using thinner layers. While thinner TFB ILs had lower luminance values than the thicker ones, the drop in luminance was not as large as would be expected if the primary function of the IL was to reduce exciton quenching by PEDOT:PSS through physically removing the RZ away from the anode, therefore other parameters, such as a large energy gap are also important in blocking excitons at the IL/light emitting polymer interface.

V. CONCLUSIONS

The aim of this work was to shed light on the origin of the large increases in efficiency that are found when a TFB IL is used at the anode-side of F8BT PLEDs. We investigated a broad range of IL parameters to establish which of them had the most significant effect. When we varied the IL material we found minimal changes in current densities, but large variations in the luminance. The changes in the luminance do not correlate with the hole injection barriers in the PLED structure nor with the current densities in the hole-only diode structure. Neither is a strong correlation between the luminance values and the IL's electron blocking barrier found. PLEDs with ILs doped with 7% F_4TCNQ by weight did not display higher efficiencies nor did the corresponding hole-only diode structures reveal a correlation between their current densities and device efficiency. However, there was evidence to suggest that exciton blocking plays a major role. Reducing the thickness of the IL below the exciton diffusion length was shown to reduce efficiencies by a small amount.

The most important role of the TFB IL in increasing PLED efficiencies in F8BT devices was therefore found to be exciton blocking *via* the differences in the energy gap between the LEP and the IL. PLED luminance showed an exponential correlation to the IL-LEP energy gap difference both experimentally and in 3D KCM simulations. The importance of exciton blocking is likely of particular importance in thin-film F8BT PLEDs because the singlet RZ is adjacent to the anode in such devices. The implications of this study are that ILs, hole injection layers and electron injecting layers in organic LEDs with active layers <100 nm should, as a first consideration, have very large energy gaps in order to limit losses from exciton quenching. Electrode quenching strongly affects the excitons created adjacent to the charge injection layers. Some small molecule OLEDs have active layer thicknesses in the region of 30 nm, which could lead to large losses due to quenching. Sourcing materials for hole and electron injection layers with larger energy gaps than currently used is therefore expected to increase PLED and OLED efficiencies.

ACKNOWLEDGMENTS

The authors thank the UK Engineering and Physics Sciences Research Council (EPSRC) (Grant No. EP/P505550/1, EP/G031088/1) the European Union Erasmus Mundus Program, and the Korean World Class Universities Project (Grant No. R32-10051) for funding and studentships. We also thank Cambridge Display Technology for supplying polymer materials and the University of Bath Aquila High Performance Computer on which the modelling was done. DDCB is the Lee-Lucas Professor of Experimental Physics.

[1]N. Tokmoldin, N. Griffiths, D. D. C. Bradley, and S. A. Haque, Adv. Mater. **21**, 3475 (2009).
[2]M. Sessolo and H. J. Bolink, Adv. Mater. **23**, 1829 (2011).
[3]D. Kabra, L. P. Lu, M. H. Song, H. J. Snaith, and R. H. Friend, Adv. Mater. **22**, 3194 (2010).
[4]J. S. Kim, R. H. Friend, and F. Cacialli, J. Appl. Phys. **86**, 2774 (1999).
[5]J. S. Kim, R. H. Friend, I. Grizzi, and J. H. Burroughes, Appl. Phys. Lett. **87**, 023506 (2005).
[6]D.-Y. Chung, D.-S. Leem, D. D. C. Bradley, and A. J. Campbell, Appl. Phys. Lett. **98**, 103306 (2011).
[7]R. Jin, P. A. Levermore, J. Huang, X. Wang, D. D. C. Bradley, and J. C. DeMello, Phys. Chem. Chem. Phys. **11**, 3455 (2009).
[8]T. M. Brown, J. S. Kim, R. H. Friend, F. Cacialli, R. Daik, and W. J. Feast, Appl. Phys. Lett. **75**, 1679 (1999).
[9]P. A. Levermore, X. Wang, L. Chen, and D. D. C. Bradley, SID Int. Symp. Dig. Tech. Pap. **39**, 1989 (2008).
[10]M. Roberts, K. Asada, M. Cass, C. Coward, S. King, A. Lee, M. Pintani, M. Ramon, and C. Foden, Proc. SPIE **7722**, 77220C (2010).
[11]X. H. Yang, F. Jaiser, B. Stiller, D. Neher, F. Galbrecht, and U. Scherf, Adv. Funct. Mater. **16**, 2156 (2006).
[12]M. J. Harding, D. Poplavskyy, V.-E. Choong, A. J. Campbell, and F. So, Org. Electron. **9**, 183 (2008).
[13]B. D. Chin, N. S. Kang, J.-W. Yu, S. Mu Jo, and J. Y. Lee, J. Appl. Phys. **102**, 024506 (2007).
[14]P. Lane, P. Brewer, J. Huang, D. Bradley, and J. DeMello, Phys. Rev. B **74**, 125320 (2006).
[15]Y. Hou, M. Koeberg, and D. D. C. Bradley, Synth. Met. **139**, 859 (2003).

[16]M. Redecker, D. D. C. Bradley, M. Inbasekaran, W. W. Wu, and E. P. Woo, Adv. Mater. **11**, 241 (1999).
[17]J. H. Burroughes, J.-S. Kim, and K.-H. Yim, European patent application 2059959 (A2) (20 May 2007).
[18]P. A. Levermore, R. Jin, X. Wang, J. C. de Mello, and D. D. C. Bradley, Adv. Funct. Mater. **19**, 950 (2009).
[19]L. Bürgi, T. J. Richards, R. H. Friend, and H. Sirringhaus, J. Appl. Phys. **94**, 6129 (2003).
[20]K.-H. Yim, G. L. Whiting, C. E. Murphy, J. J. M. Halls, J. H. Burroughes, R. H. Friend, and J. S. Kim, Adv. Mater. **20**, 3319 (2008).
[21]A. J. Campbell, D. D. C. Bradley, and H. Antoniadis, Appl. Phys. Lett. **79**, 2133 (2001).
[22]J. Zaumseil, C. L. Donley, J. S. Kim, R. H. Friend, and H. Sirringhaus, Adv. Mater. **18**, 2708 (2006).
[23]N. Koch, A. Elschner, and R. L. Johnson, J. Appl. Phys. **100**, 024512 (2006).
[24]J. D. A. Lin, O. V. Mikhnenko, J. Chen, Z. Masri, A. Ruseckas, A. Mikhailovsky, R. P. Raab, J. Liu, P. W. M. Blom, M. A. Loi, C. J. García-Cervera, I. D. W. Samuel, and T.-Q. Nguyen, Mater. Horiz. **1**, 280 (2014).
[25]M. Stevens, C. Silva, D. Russell, and R. Friend, Phys. Rev. B **63**, 165213 (2001).
[26]L.-L. Chua, J. Zaumseil, J.-F. Chang, E. C.-W. Ou, P. K.-H. Ho, H. Sirringhaus, and R. H. Friend, Nature **434**, 194 (2005).
[27]P. J. Brewer, A. J. DeMello, J. C. DeMello, P. A. Lane, D. D. C. Bradley, R. Fletcher, and J. O'Brien, J. Appl. Phys. **99**, 114502 (2006).
[28]P. A. Levermore, L. Chen, X. Wang, R. Das, and D. D. C. Bradley, Adv. Mater. **19**, 2379 (2007).
[29]D. Poplavskyy, W. Su, and F. So, J. Appl. Phys. **98**, 014501 (2005).
[30]D. Poplavskyy and F. So, J. Appl. Phys. **99**, 033707 (2006).
[31]R. G. E. Kimber, E. N. Wright, S. E. J. O'Kane, A. B. Walker, and J. C. Blakesley, Phys. Rev. B **86**, 235206 (2012).
[32]R. G. E. Kimber, A. B. Walker, G. E. Schröder-Turk, and D. J. Cleaver, Phys. Chem. Chem. Phys. **12**, 844 (2010).
[33]P. K. Watkins, A. B. Walker, and G. L. B. Verschoor, Nano Lett. **5**, 1814 (2005).
[34]J.-L. Brédas, D. Beljonne, V. Coropceanu, and J. Cornil, Chem. Rev. **104**, 4971 (2004).
[35]I. Hulea, H. Brom, A. Houtepen, D. Vanmaekelbergh, J. Kelly, and E. Meulenkamp, Phys. Rev. Lett. **93**, 166601 (2004).
[36]S. Athanasopoulos, E. V. Emelianova, A. B. Walker, and D. Beljonne, Phys. Rev. B **80**, 195209 (2009).
[37]I. Fishchuk, D. Hertel, H. Bässler, and A. Kadashchuk, Phys. Rev. B **65**, 125201 (2002).
[38]J. Hill, S. Y. Heriot, O. Worsfold, T. H. Richardson, A. M. Fox, and D. D. C. Bradley, Phys. Rev. B **69**, 041303 (2004).
[39]Y. Zhang and S. R. Forrest, Phys. Rev. Lett. **108**, 267404 (2012).
[40]K. A. Neyts, J. Opt. Soc. Am. A **15**, 962 (1998).
[41]J. Staudigel, M. Stößel, F. Steuber, and J. Simmerer, J. Appl. Phys. **86**, 3895 (1999).
[42]K.-H. Yim, R. Friend, and J. S. Kim, J. Chem. Phys. **124**, 184706 (2006).
[43]A. C. Arias, J. D. MacKenzie, R. Stevenson, J. J. M. Halls, M. Inbasekaran, E. P. Woo, D. Richards, and R. H. Friend, Macromolecules **34**, 6005 (2001).
[44]R. Stevenson, A. C. Arias, C. Ramsdale, J. D. MacKenzie, and D. Richards, Appl. Phys. Lett. **79**, 2178 (2001).
[45]A. Morteani, P. Sreearunothai, L. Herz, R. Friend, and C. Silva, Phys. Rev. Lett. **92**, 247402 (2004).
[46]R. G. Sharpe and R. E. Palmer, J. Phys. Condens. Matter **8**, 329 (1996).
[47]A. Kokil, K. Yang, and J. Kumar, J. Polym. Sci. Part B Polym. Phys. **50**, 1130 (2012).
[48]J. C. Blakesley, F. A. Castro, W. Kylberg, G. F. A. Dibb, C. Arantes, R. Valaski, M. Cremona, J. S. Kim, and J. S. Kim, Org. Electron. **15**(6), 1263 (2014).
[49]R. Khan, D. Poplavskyy, T. Kreouzis, and D. Bradley, Phys. Rev. B **75**, 035215 (2007).
[50]H. H. Fong, A. Papadimitratos, and G. G. Malliaras, Appl. Phys. Lett. **89**, 172116 (2006).
[51]Y. Kim, S. Cook, S. A. Choulis, J. Nelson, J. R. Durrant, and D. D. C. Bradley, Chem. Mater. **16**, 4812 (2004).
[52]W. Gao and A. Kahn, Org. Electron. **3**, 53 (2002).
[53]E. F. Aziz, A. Vollmer, S. Eisebitt, W. Eberhardt, P. Pingel, D. Neher, and N. Koch, Adv. Mater. **19**, 3257 (2007).
[54]D. D. C. Bradley and R. H. Friend, J. Phys. Condens. Matter **1**, 3671 (1989).
[55]P. A. Levermore, *A Study of Poly(3,4-Ethylenedioxythiophene) and Related Organic Light Emitting Device Applications* (Imperial College London, 2008).
[56]A. Weller, "Singlet- and triplet-state exciplexes," in *The Exciplex* (Academic Press, New York, 1975).